Structural Engineering and Mechanics, *Vol. 59, No. 3 (2016) 431-454*
DOI: http://dx.doi.org/10.12989/sem.2016.59.3.431

Nonlinear static and vibration analysis of Euler-Bernoulli composite beam model reinforced by FG-SWCNT with initial geometrical imperfection using FEM

M. Mohammadimehr* and S. Alimirzaei

Department of Solid Mechanics, Faculty of Mechanical Engineering, University of Kashan, P.O. Box: 87317-51167, Kashan, Iran

(Received May 21, 2015, Revised March 29, 2016, Accepted April 11, 2016)

Abstract. In this paper, the nonlinear static and free vibration analysis of Euler-Bernoulli composite beam model reinforced by functionally graded single-walled carbon nanotubes (FG-SWCNTs) with initial geometrical imperfection under uniformly distributed load using finite element method (FEM) is investigated. The governing equations of equilibrium are derived by the Hamilton's principle and von Karman type nonlinear strain-displacement relationships are employed. Also the influences of various loadings, amplitude of the waviness, UD, USFG, and SFG distributions of carbon nanotube (CNT) and different boundary conditions on the dimensionless transverse displacements and nonlinear frequency ratio are presented. It is seen that with increasing load, the displacement of USFG beam under force loads is more than for the other states. Moreover it can be seen that the nonlinear to linear natural frequency ratio decreases with increasing aspect ratio (*h/L*) for UD, USFG and SFG beam. Also, it is shown that at the specified value of (*h/L*), the natural frequency ratio increases with the increasing the values amplitude of waviness while the dimensionless nonlinear to linear maximum deflection decreases. Moreover, with considering the amplitude of waviness, the stiffness of Euler-Bernoulli beam model reinforced by FG-CNT increases. It is concluded that the *R* parameter increases with increasing of volume fraction while the rate of this parameter decreases. Thus one can be obtained the optimum value of FG-CNT volume fraction to prevent from resonance phenomenon.

Keywords: nonlinear static and free vibration analysis; Euler-Bernoulli composite beam model; various distribution patterns of SWCNTs; geometrical imperfection; FEM

1. Introduction

A functionally graded material (FGM) is described by material variant from one to another surface for the optimum distribution of component materials. These materials are used widely in many fields, such as aerospace technology, automobiles, electronics, optics, chemistry, biomedical engineering, nuclear engineering and mechanical engineering.

So many researches in the field of vibration, statics and buckling analysis are done by researchers on them (Lau *et al*. 2004). The mixed finite element models of beams and plates were

*Corresponding author, Ph.D., E-mail: mmohammadimehr@kashanu.ac.ir

http://www.techno-press.org/?journal=sem&subpage=8 ISSN: 1225-4568 (Print), 1598-6217 (Online)

developed more than two decades ago by (Putcha and Refined 1986, Reddy 1987) to overcome the drawbacks of the displacement based models. Wave propagation analysis in nonlinear curved single-walled carbon nanotubes (SWCNTs) based on nonlocal elasticity theory is investigated by Wang *et al*. (2015). The effects of the geometrical nonlinearity, the initial geometrical imperfection, temperature change and magnetic field on the flexural and shear wave frequencies are investigated. Liew and co-worker (2015) investigated mechanical analysis of functionally graded carbon nanotube reinforced composite. They attempt to identify and highlight topics relevant to functionally graded carbon nanotube reinforced composite (FG-CNTRC) and review the recent research works that have been reported. Eltaher and co-workers (2014) studied the nonlinear free vibration of uniform cross section FG beam based on the nonlocal Timoshenko beam theory (TBT). Their obtained the numerical results are reflected the significant effect of neutral axisposition, material distribution profile, and the nonlocality parameter on the fundamental frequencies of nano-Timoshenko beams. Free vibration and buckling analysis of Timoshenko beams reinforced by SWCNTs is studied by Yas and Samadi (2012). Their results illustrated that several parameters such as boundary conditions, volume fraction of nanotube and foundation stiffness are effective in free vibration and buckling characteristics of beam. Static and nonlinear vibration analysis of micro beams based on elastic foundation using Euler-Bernoulli beam theory (EBBT) is investigated by Simsek (2014). He considered the effects of the length scale parameter and the stiffness coefficients of the nonlinear foundation on the static deflection and the ratio of nonlinear to linear frequency. Mohammadimehr and Rahmati (2013) presented the electro-thermo-mechanical nonlocal axial vibration analysis of single-walled boron-nitride nano-rods (SWBNNRs) under electric excitation. They obtained the constitutive equation for the nano-rods under electro-thermo-mechanical loadings, then they discussed about effects of the aspect ratio, small scale parameter, clamped-clamped and clamped-free boundary conditions on the natural frequency. Nonlinear thermal buckling behavior of functionally graded (FG) plates using an efficient sinusoidal shear deformation theory is illustrated by Bouiadjra *et al*. (2013). Their numerical results presented to study the efficient sinusoidal shear deformation theory that is importance and accuracy in comparison to other theory. Ansari and Ramezan-nezhad (2011) in one of their recent publications studied the nonlinear vibrations of embedded multi-walled carbon nanotubes in thermal environments based on the nonlocal Timoshenko beam model. They obtained the effects of small-scale parameter; nanotube geometries, temperature change and the elastic medium on the natural frequency. Farshidianfar and Soltani (2012) exploited an efficient nonlinear vibrational model for fluid-conveying CNT with geometrical imperfection. Their obtained results revealed that the imperfection of the nanotube at high flow velocities makes the model severely nonlinear, especially when considering the nonlocal effects. Nonlinear vibration of embedded SWCNT with geometrical imperfection under harmonic load based on nonlocal TBT is studied by Wang *et al*. (2013).Their results showed that the above mentioned effects have influences on the dynamic behaviour of the SWCNT. Li (2013) investigated size-dependent thermal behaviors of axially traveling nano-beams based on a strain gradient theory. They considered the effects of strain gradient nano-scale parameter, temperature change; shape parameter and axial traction on the natural frequencies and discussed through some numerical examples. It is concluded that the factors mentioned above significantly influence the dynamic behaviors of an axially traveling nano-beam. Ghorbanpour and co-workers (2012) investigated nonlinear vibration of embedded single-walled boron nitride nanotubes (SWBNNTs) based on nonlocal TBT using differential quadrature method (DQM). They concluded that imposing a direct electric potential in axially polarized direction causes decreasing fundamental frequency and applying it in reverse direction

increases it. Rahmati and Mohammadimehr (2014) investigated the vibration analysis of non-uniform and non-homogeneous boron nitride nanorod (BNNR) embedded in an elastic medium under combined loadings using DQM. They indicated that the non-dimensional frequency ratio of nonhomogeneous BNNR decreases with the presence of electro-thermal loadings, and their effect on the nondimensional frequency ratio is higher in short nanorods and high nonlocal parameter. In the other work, based on strain gradient theory, Mohammadimehr *et al*. (2015a) presented the free vibration analysis of tapered viscoelastic micro-rod resting on visco-Pasternak foundation. They assumed the material properties of micro-rod to be the visco-elastic and modeled as the Kelvin-Voigt. Using Hamilton's principle and energy method, they obtained the governing equation of motion of viscoelastic micro-rods, then this equation solved using DQM for different boundary conditions. Also, Mohammadimehr *et al*. (2016a) illustrated the size dependent effect on the buckling and vibration analysis of double-bonded nanocomposite piezoelectric plate reinforced by boron nitride nanotube (BNNT) based on modified couple stress theory. The results of their research showed that the critical buckling load decreases with an increase in the dimensionless material length scale parameter. Large deflection analysis of edge cracked simply supported beams is studied by Akbas (2015). In this study, the effects of the location of crack and the depth of the crack on the non-linear static response of the beam are investigated in detail. The relationships between deflections, end rotational angles, end constraint forces, deflection configuration, Cauchy stresses of the edge- cracked beams and load rising are illustrated in nonlinear case. Also, the difference between the geometrically linear and nonlinear analysis of edge-cracked beam is presented. Dynamic analysis of FG nano-composite beams reinforced by randomly oriented CNTunder the action of moving load is investigated by Yas and Heshmati (2012). Their obtained results indicated that a CNT-reinforced composite can possibly reach superior vibrational properties only if the CNTs are controlled to be aligned in the whole material. Ranjan (2011) studied the nonlinear finite element analysis of bending of straight beams using hp-spectral approximations. His results compared with both analytical and nonlinear finite element solutions from literature that have excellent agreement with them.

In this paper, the nonlinear bending and free vibration analysis of Euler-Bernoulli composite beam model reinforced by FG-SWCNTs with geometrical imperfection under uniformly distributed load using FEM is considered for various distributions of CNTs and different boundary conditions. Based on the Hamilton's principle and von Karman type, the governing equations of equilibrium are obtained. Also the influences of various loadings, amplitude of the waviness, UD, USFG, and SFG distributions of CNT and different boundary conditions on the dimensionless transverse deflection and nonlinear frequency ratio are illustrated.

2. Material properties of CNTRC beams

The nano-composite beam has an initial sinusoidal curvature described by (Wang *et al*. 2013)

$$w_0(\mathrm{x}) = \mu \sin(\frac{\pi \mathrm{x}}{l}) \tag{1}$$

where μ is the amplitude of the waviness.

The mixture of rule for FG nano-composite beam reinforced by SWCNT is obtained by the following equation (Yas and Samadi 2012)

$$V_{CNT} + V_m = 1 \tag{2}$$

where V_{CNT} and V_m are CNT and matrix volume fractions, respectively. V_{CNT} is defined for different types of CNT distribution. In this paper, three kinds of CNT distribution are assumed as (Yas and Samadi 2012):

Uniform distribution (UD)

$$V_{CNT} = \bar{V}_{CNT} \tag{3}$$

Unsymmetrical functionally graded distribution of CNT (USFG)

$$V_{CNT}(z) = \left(1 - \frac{2z}{h}\right)\bar{V}_{CNT} \tag{4}$$

Symmetrically linear distribution of CNT (SFG)

$$V_{CNT}(z) = 2\left(\frac{2|z|}{h}\right)\bar{V}_{CNT} \tag{5}$$

where $\bar{V}_{CNT}$ is

$$\bar{V}_{CNT} = \frac{W_{CNT}}{W_{CNT} + (\frac{\rho_{CNT}}{\rho_m}) - (\frac{\rho_{CNT}}{\rho_m})W_{CNT}} \tag{6}$$

W_{CNT}, ρ_{CNT} and ρ_m are mass fraction of CNT, density of CNT and matrix, respectively.

Similarly, Poisson's ratio, mass density and Young's modulus in terms of Euler-Bernoulli composite beam model reinforced by FG-CNTs can be expressed as (Heshmati and Yas 2013, Mohammadimehr *et al*. 2016b, Mohammadimehr and Mostafavifar 2016)

$$\begin{aligned} \rho(z) &= V_{CNT}\rho_{CNT} + V_m\rho_m \\ \nu(z) &= V_{CNT}\nu_{CNT} + V_m\nu_m \\ E(z) &= V_{CNT}E_{CNT} + V_mE_m \end{aligned} \tag{7}$$

3. Theory and formulations

3.1 Equations of motion

The Euler-Bernoulli theory (EBT) is based on the assumption that a straight line transverse to the axis of the beam remains straight, inextensible, and normal to the mid-plane after deformation. These assumptions amount to neglecting the Poisson ratio effect and the transverse strains. The displacement field for EBT beams can be written as the following form

$$\begin{aligned} u_1(x,z) &= u(x) - z\frac{\partial w(x,z)}{\partial x} \\ u_2(x,z) &= 0\ ,\ u_3(x,z) = w(x) \end{aligned} \tag{8}$$

where (u_1, u_2, u_3) is the total displacements along the three coordinate directions (x,y,z), u and w denote the axial and transverse displacements of a point on the neutral axis, respectively. The nonlinear strain-displacement relationships of uniform beam with initial geometrical imperfection

undergoing large deflections are obtained as follows (Wang *et al*. 2013, Li 2014)

$$\varepsilon_{xx} = \frac{\partial u}{\partial x} - z\frac{\partial^2 w}{\partial x^2} + \frac{1}{2}(\frac{\partial w}{\partial x})^2 + \frac{\partial w}{\partial x}\frac{\partial w_0}{\partial x} \tag{9}$$

where w_0 is the initial geometrical imperfection. For imperfect beams, the initial geometrical imperfection w_0 is assumed to be the form similar to the deformed shape with w, and have $w_0=\mu w$, μ is the imperfection parameter (Li 2014).The strain and kinetic energy of the Euler-Bernoulli composite beam model reinforced by FG-CNTs are as follows

$$\begin{aligned} T &= \frac{1}{2}\int_0^L\int_A \rho(z)(\dot{u}_1^2 + \dot{u}_2^2 + \dot{u}_3^2)dAdx \\ S &= \frac{1}{2}\int_0^L\int_A (\sigma_{xx}\varepsilon_{xx})dAdx \end{aligned} \tag{10a}$$

$$\sigma_{xx} = E(z)\varepsilon_{xx} \tag{10b}$$

where σ_{xx} is the normal stress of nano-composite beam. Also T and S denote the kinetic energy and strain energy, respectively.

The equilibrium equations of CNTs can be obtained by the energy principle and the variational approach. The variation strain energy can be calculated as

$$\begin{aligned} &\delta S = \int_0^L\int_A (\sigma_{xx}\delta\varepsilon_{xx})dAdx \\ &\delta S = \int_A [N_x\left(\frac{\partial \delta u}{\partial x}\right) + 2\mu N_x\left(\frac{\partial w}{\partial x}\frac{\partial \delta w}{\partial x}\right) - M_X\left(\frac{\partial^2 \delta w}{\partial x^2}\right) \\ &+N_x\left(\frac{\partial w}{\partial x}\frac{\partial \delta W}{\partial x}\right)]dA \end{aligned} \tag{11}$$

where N_x and M_x are the resultant axial force and moment, respectively which is defined as

$$\{N_x, M_x\} = \int_{-h/2}^{h/2} \sigma_x(1, z)dz \tag{12}$$

Substituting Eq. (12) into Eq. (11), one can be obtained the following equations (for details see Reddy 2004)

$$\int_A [\frac{\partial \delta u}{\partial x}\left(A_{11}\frac{\partial u}{\partial x} - B_{11}\frac{\partial^2 \delta w}{\partial x^2} + (\mu + \frac{1}{2})\mathrm{A}_{11}(\frac{\partial w}{\partial x})^2\right)]dA = 0 \tag{13}$$

$$\begin{aligned} &\int_A [\frac{\partial w}{\partial x}\ \frac{\partial \delta w}{\partial x}\begin{pmatrix} A_{11}(2\mu+1)\frac{\partial u}{\partial x} - B_{11}(2\mu+1)\frac{\partial^2 w}{\partial x^2} \\ +(2\mu^2 + 2\mu + \frac{1}{2})\mathrm{A}_{11}(\frac{\partial w}{\partial x})^2 \end{pmatrix}]\mathrm{dx} \\ &-\int \frac{\partial^2 \delta w}{\partial x^2}[B_{11}\frac{\partial u}{\partial x} + B_{11}(\mu + \frac{1}{2})(\frac{\partial w}{\partial x})^2 - \mathrm{D}_{11}\frac{\partial^2 w}{\partial x^2}]\mathrm{dx} = 0 \end{aligned} \tag{14}$$

where stiffness coefficient are considered as

$$[\mathrm{A}_{11}\ \mathrm{B}_{11}\ \mathrm{D}_{11}]=\int_{-\frac{h}{2}}^{\frac{h}{2}} E(z)[1\ z\ z^2]dz \tag{15}$$

Also the variation kinetic energy can be calculated as

$$\begin{aligned}&\delta T=\int_0^L\int_A \rho(z)(\ddot{u}_1\,\delta u_1+\ddot{u}_3\,\delta u_3)dA\,dx\\&\int_0^L\int_A \rho(z)\left[\left(\delta u-z\,\delta w_{,x}\right)\left(\ddot{u}-z\,\ddot{w}_{,x}\right)+\ddot{w}\,\delta w\right]dA\,dx\\&[\mathrm{I}_0\ \mathrm{I}_1\ \mathrm{I}_2]=\int_{-\frac{h}{2}}^{\frac{h}{2}}\rho(z)[1\ z\ z^2]\,dz\end{aligned} \tag{16}$$

3.2 Maxwell's equation

For Euler-Bernoulli composite beam model reinforced by FG-SWCNT subjected to a magnetic field, *H*, the exerted body force can be calculated as (Narendar *et al.* 2012, Mohammadimehr *et al.* 2015b)

$$\begin{aligned}&h=Curl\,(\mathrm{U}\times\mathrm{H})=\nabla\times\begin{vmatrix}u & 0 & w\\ H_x & 0 & 0\end{vmatrix}=\nabla\times(0,wH_x,0)=\begin{vmatrix}\frac{\partial}{\partial x} & \frac{\partial}{\partial y} & \frac{\partial}{\partial z}\\ 0 & wH_x & 0\end{vmatrix}=\\&(-\frac{\partial}{\partial z}wH_x,0,\frac{\partial}{\partial x}wH_x)=(0,0,\frac{\partial}{\partial x}wH_x)\end{aligned} \tag{17}$$

For simplifying the analysis, a longitudinal vector is considered as H= (H_x, 0, 0). The current density (J) and the Maxwell equations are given by

$$J=Curl\,(h)=\nabla\times h=\begin{vmatrix}\frac{\partial}{\partial x} & \frac{\partial}{\partial y} & \frac{\partial}{\partial z}\\ 0 & 0 & \frac{\partial}{\partial x}wH_x\end{vmatrix}=(0,-\frac{\partial}{\partial x}(\frac{\partial}{\partial x}wH_x),0) \tag{18}$$

$$\mathrm{f}=\mu_0\times(\mathrm{J}\times h)=\mu_0\times\begin{vmatrix}0 & -\frac{\partial}{\partial x}\left(\frac{\partial}{\partial x}wH_x\right) & 0\\ H_x & 0 & 0\end{vmatrix}=\mu_0 H_x^2\frac{\partial}{\partial x}(\frac{\partial w}{\partial x})=\mu_0 H_x^2\frac{\partial^2 w}{\partial x^2} \tag{19}$$

where μ_0 is the magnetic field permeability.

Therefore the component of Lorentz forces along the *x*, *y* and *z* directions are

$$f_x=0,\ f_y=0,\ f_z=\mu_0 H_x^2\left(\frac{\partial^2 w}{\partial x^2}\right) \tag{20}$$

The variation of work done due to the external load such as magnetic field and distribution

load, for nano-composite beam is described by

$$\delta W_{Lorentz} = \delta W_{Lorentz} + \delta W_{load} = -\int_A f_z \ \delta w \ dA - \int_A q \ \delta w \ dA \tag{21}$$

where f_z and q are the work done due to the external load such as magnetic field and uniformly distributed load, respectively.

In this investigation different boundary conditions of the beams such as simply-simply (S-S), simply-hinged (S-H), clamped-clamped (C-C), camped-simply (C-S) are considered. These conditions are described as

$$\begin{aligned} &\text{clamped (C):} && u = w = \frac{dw}{dx} = 0 \\ &\text{hinged (H):} && w = 0, \ \ M_x = 0 \\ &\text{simply support (S):} && u = w = 0, \ M_x = 0 \end{aligned} \tag{22}$$

3.3 Finite Element Method (FEM)

In this paper, FEM is used to solve the governing equations of CNTRC beams. According to FEM the axial displacement *u(x)* and transverse deflection *w(x)* are interpolated as (Reddy 2004)

$$u(\mathrm{x}) = \sum_{J=1}^{2} N_{uj} \ u_j \ , \ w(\mathrm{x}) = \sum_{J=1}^{4} N_{wj} \ w_j \tag{23}$$

Here N_{uj}, N_{wj} are the exact shape functions for axial, transverse and rotational degrees-of-freedom, respectively.

Substituting Eq. (23), and $\delta w_0(x)=N_{wi}(x)$ and $\delta u_0(x)=N_{ui}(x)$ into the Eqs. (13)-(14) and (16) we obtain

$$\begin{aligned} &\sum_{j=1}^{2} K_{ij}^{11} u_j + \sum_{J=1}^{4} K_{iJ}^{12} w_J - F_i^1 = 0 \quad i, j = 1,2 \\ &\sum_{J=1}^{2} K_{Ij}^{21} u_j + \sum_{J=1}^{4} K_{IJ}^{22} w_j - F_I^2 = 0 \quad I, J = 1,2,3,4 \end{aligned} \tag{24}$$

where

$$K_{ij}^{11} = \int_{x_a}^{x_b} A(\mathrm{z}) \ \frac{dN_{ui}}{dx} \ \frac{dN_{uj}}{dx} \ dx \ ,$$

$$K_{iJ}^{12} = \frac{1}{2} \int_{x_a}^{x_b} A(\mathrm{z}) \ (2\mu + 1) \ \frac{dw}{dx} \frac{dN_{ui}}{dx} \ \frac{dN_{wJ}}{dx} \ dx - \int_{x_a}^{x_b} \mathrm{B}(\mathrm{z}) \ \frac{dN_{ui}}{dx} \ \frac{d^2 N_{wJ}}{dx^2} \ dx$$

$$K_{Ij}^{21} = \int_{x_a}^{x_b} A(\mathrm{z}) \ (2\mu + 1) \ \frac{dw}{dx} \frac{dN_{wI}}{dx} \ \frac{dN_{uj}}{dx} \ dx - \int_{x_a}^{x_b} \mathrm{B}(\mathrm{z}) \ \frac{d^2 N_{wI}}{dx^2} \ \frac{dN_{uj}}{dx} \ \ dx$$

$$K_{IJ}^{22}=\int_{x_a}^{x_b}\mathrm{B(z)}\ (2\mu+1)\ \frac{dw}{dx}\frac{dN_{wI}}{dx}\ \frac{d^2N_{wJ}}{dx^2}\ dx+$$
$$\int_{x_a}^{x_b}A(\mathrm{z})\ (2\mu^2+2\mu+\frac{1}{2})\ (\frac{dw}{dx})^2\ \frac{dN_{wI}}{dx}\ \frac{dN_{wJ}}{dx}\ dx-$$
$$\int_{x_a}^{x_b}\mathrm{B(z)}\ (\mu+\frac{1}{2})\ \frac{dw}{dx}\frac{d^2N_{wI}}{dx^2}\frac{dN_{wJ}}{dx}\ \ dx+\int_{x_a}^{x_b}D(\mathrm{z})\frac{d^2N_{wI}}{dx^2}\frac{d^2N_{wJ}}{dx^2}\ \ dx-$$
$$b\int_{x_a}^{x_b}\mu_0\,H_x^2\,\mathrm{N}_{wI}\,\frac{d^2N_{wJ}}{dx^2}\,dx \tag{25}$$

Also

$$M_{11}=\int_{x_a}^{x_b}I_0\ [N_{ui}]\,[N_{uj}]dx\ \ ,\ M_{12}=\int_{x_a}^{x_b}I_1\ [N_{ui}]\,\frac{d\,[N_{wJ}]}{dx}\,dx,$$
$$M_{21}=\int_{x_a}^{x_b}I_1\ \frac{d\,[N_{wI}]}{dx}\,[N_{uj}]\,dx, \tag{26}$$
$$M_{22}=\int_{x_a}^{x_b}I_3\ \frac{d\,[N_{wI}]}{dx}\,\frac{d\,[N_{wJ}]}{dx}\,dx+\int_{x_a}^{x_b}I_0\ [N_{wI}]\,[N_{wJ}]\,dx$$

The consistent force array is given by

$$\{\mathrm{F}\}=\int_0^L q\,N_w\,dx \tag{27}$$

The consistent load vector for the uniformly distributed load (q) is calculated by substituting the shape functions into Eq. (27).

3.4 Linearization procedure

The linearization process can be accomplished with type two techniques, namely the Picard (direct iteration procedure) or the Newton-Raphson's method. For checking the convergence behaviour of both the methods of linearization's with hp-spectral methods both of these were implemented. Some of the advantages of the Newton-Raphson method are a faster convergence rate. The linearized problem with the Newton's method is represented as follows (Reddy 2004)

$$\left[k_1(\{\Delta\}^{(\mathrm{r}-1)})\right]\{\Delta\}^r=-\left\{\mathrm{R}(\{\Delta\}^{(\mathrm{r}-1)})\right\}=\{F\}-\left(\left[k^e\right]\{\Delta^e\}\right)^{(\mathrm{r}-1)} \tag{28}$$

where the tangent stiffness matrix [k_1] associated with the Euler-Bernoulli beam element is calculated as follows

$$[k_1]=-\left(\frac{\partial\{\mathrm{R}\}}{\partial\{\Delta\}}\right)^{(\mathrm{r}-1)} \tag{29}$$

The solution at the rth iteration is then given by: $\{\Delta\}r=\{\Delta\}(r-1)+\{\delta\Delta\}$

For the check of the convergence criterion, it can be computed by using the increment of the solutions vector, i.e., $\{\delta\Delta\}$, as follows

$$\sqrt{\frac{\sum_{I=1}^{N}(\Delta U_I)^2}{\sum_{I=1}^{N}(U_I^{(r)})^2}} < \hat{\lambda} \tag{30}$$

It is noted that the calculations were carried out on a 36-digit precision computer and iterated until all percentage relative errors changed by less than $\hat{\lambda} = 0.00001$ between iterations (Reddy 2004):

Although the direct stiffness matrix [k] is unsymmetrical, it can be shown that the tangent stiffness matrix [k_1] is symmetric. Therefore

$$\begin{aligned}
k_{1\ ij}^{11} &= k_{ij}^{11} + \sum_{p=1}^{2}\left(\frac{\partial k_{ip}^{11}}{\partial u_j}\right)u_p + \sum_{p=1}^{4}\left(\frac{\partial k_{ip}^{12}}{\partial u_j}\right)w_p = k_{ij}^{11} \\
k_{1\ iJ}^{12} &= k_{iJ}^{12} + \sum_{p=1}^{2}\left(\frac{\partial k_{ip}^{11}}{\partial w_J}\right)u_p + \sum_{p=1}^{4}\left(\frac{\partial k_{ip}^{12}}{\partial w_J}\right)w_p = k_{iJ}^{12} + \frac{1}{2}\int_{x_a}^{x_b} A(z)\ (2\mu+1)\ \frac{dw}{dx}\frac{dN_{ui}}{dx}\frac{dN_{wJ}}{dx}\,dx \\
k_{1\ IJ}^{22} &= k_{IJ}^{22} + \sum_{p=1}^{2}\left(\frac{\partial k_{Ip}^{21}}{\partial w_J}\right)u_p + \sum_{p=1}^{4}\left(\frac{\partial k_{Ip}^{22}}{\partial w_J}\right)w_p = k_{IJ}^{22} + \int_{x_a}^{x_b} B(z)\ (2\mu+1)\ \frac{d^2w}{dx^2}\frac{dN_{wI}}{dx}\frac{dN_{wJ}}{dx}\,dx + \\
&\int_{x_a}^{x_b} A(z)\ (4\mu^2+4\mu+1)\ (\frac{dw}{dx})^2\frac{dN_{wI}}{dx}\frac{dN_{wJ}}{dx}\,dx - \int_{x_a}^{x_b} B(z)\ (\mu+\frac{1}{2})\ \frac{dw}{dx}\frac{d^2N_{wI}}{dx^2}\frac{dN_{wJ}}{dx}\ dx + \\
&\int_{x_a}^{x_b} A(z)\ (2\mu+1)\ \frac{du}{dx}\ \frac{dN_{wI}}{dx}\frac{dN_{wJ}}{dx}dx
\end{aligned} \tag{31}$$

So the equations of motion can be obtained as matrix form

$$[M]\{\ddot{u}\}+[k]\{u\}=\{f\} \tag{32}$$

where

$$[k]=[k_{linear}]+[k_{nonlinear}] \tag{33}$$

Therefore, the total order of the stiffness and mass matrices is 6×6 which is illustrated as follows

$$\left(\begin{bmatrix} k_{11}^{11} & k_{11}^{12} & k_{12}^{12} & k_{12}^{11} & k_{13}^{12} & k_{14}^{12} \\ k_{11}^{21} & k_{11}^{22} & k_{12}^{22} & k_{12}^{21} & k_{13}^{22} & k_{14}^{22} \\ k_{21}^{21} & k_{21}^{22} & k_{22}^{22} & k_{22}^{21} & k_{23}^{22} & k_{24}^{22} \\ k_{21}^{11} & k_{21}^{12} & k_{22}^{12} & k_{22}^{11} & k_{23}^{12} & k_{24}^{12} \\ k_{31}^{21} & k_{31}^{22} & k_{32}^{22} & k_{32}^{21} & k_{33}^{22} & k_{34}^{22} \\ k_{41}^{21} & k_{41}^{22} & k_{42}^{22} & k_{42}^{21} & k_{43}^{22} & k_{44}^{22} \end{bmatrix} - \omega^2 \begin{bmatrix} M_{11}^{11} & M_{11}^{12} & M_{12}^{12} & M_{12}^{11} & M_{13}^{12} & M_{14}^{12} \\ M_{11}^{21} & M_{11}^{22} & M_{12}^{22} & M_{12}^{21} & M_{13}^{22} & M_{14}^{22} \\ M_{21}^{21} & M_{21}^{22} & M_{22}^{22} & M_{22}^{21} & M_{23}^{22} & M_{24}^{22} \\ M_{21}^{11} & M_{21}^{12} & M_{22}^{12} & M_{22}^{11} & M_{23}^{12} & M_{24}^{12} \\ M_{31}^{21} & M_{31}^{22} & M_{32}^{22} & M_{32}^{21} & M_{33}^{22} & M_{34}^{22} \\ M_{41}^{21} & M_{41}^{22} & M_{42}^{22} & M_{42}^{21} & M_{43}^{22} & M_{44}^{22} \end{bmatrix}\right)\begin{Bmatrix} u_1 \\ w_1 \\ \theta_1 \\ u_2 \\ w_2 \\ \theta_2 \end{Bmatrix} = \begin{Bmatrix} f_1 \\ f_2 \\ f_3 \\ f_4 \\ f_5 \\ f_6 \end{Bmatrix} \tag{34}$$

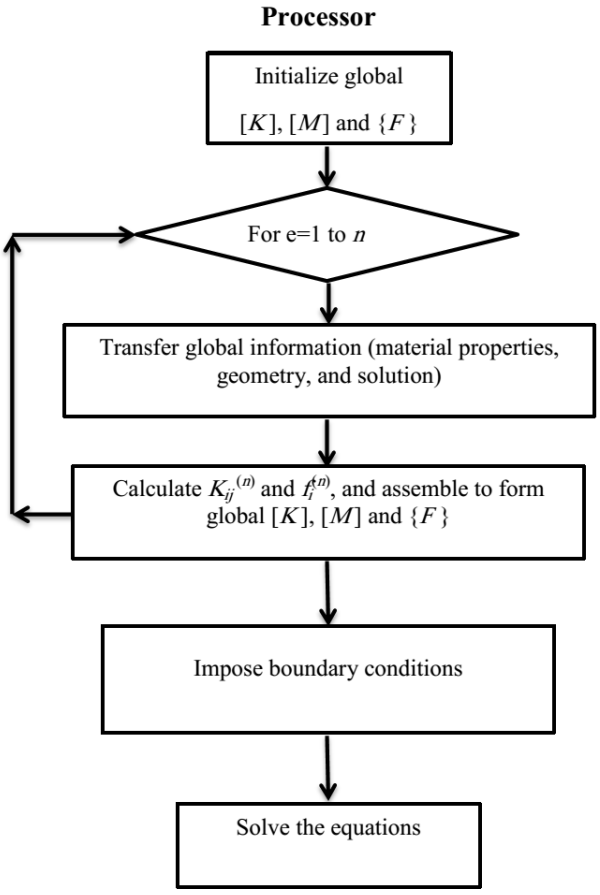

Fig. 1 A computer flow chart of Matlab software for the nonlinear finite element analysis of Euler-Bernoulli composite beam model reinforced by FG-SWCNT

The flowchart for nonlinear bending analysis of Euler-Bernoulli composite beam model reinforced by FG-SWCNT is shown in Fig. 1.

According to FEM, the stiffness and mass matrices for Timoshenko beam theory are considered as follows:

- Stiffness matrix

$$\begin{cases} K_{11}^{ij} = \int_{x_a}^{x_b} A_{11}^{0} \frac{d\,\mathrm{N}_{ui}}{dx} \frac{d\,\mathrm{N}_{uj}}{dx} dx \\ K_{12}^{ij} = \int_{x_a}^{x_b} (\mu + \frac{1}{2}) A_{11}^{0} \frac{d\,\mathrm{N}_{ui}}{dx} \frac{dN_{wj}}{dx} (\frac{dw}{dx}) dx \\ K_{13}^{ij} = \int_{x_a}^{x_b} A_{11}^{1} \frac{d\,\mathrm{N}_{ui}}{dx} \frac{d\,\mathrm{N}_{\psi j}}{dx} dx \end{cases} \tag{35a}$$

$$\begin{cases} K_{21}^{ij} = 2\int_x (\mu+\frac{1}{2})A_{11}^0 \frac{d\,\mathrm{N}_{w\,i}}{dx}\frac{d\,\mathrm{N}_{u\,j}}{dx}(\frac{\partial w}{\partial x})dx \\ K_{22}^{ij} = \int_{x_a}^{x_b} k_s B_{11}^0 \frac{d\,\mathrm{N}_{w\,i}}{dx}\frac{d\,\mathrm{N}_{w\,j}}{dx}dx + 2\int_{x_a}^{x_b}(\mu+\frac{1}{2})^2 A_{11}^0 \frac{d\,\mathrm{N}_{w\,i}}{dx}\frac{dN_{w\,j}}{dx}(\frac{dw}{dx})^2 dx \\ K_{23}^{ij} = \int_{x_a}^{x_b} k_s\, B_{11}^0 \frac{\partial\,\mathrm{N}_{w\,i}}{\partial x}N_{\psi\,j}dx + 2\int_{x_a}^{x_b}(\mu+\frac{1}{2})A_{11}^1 \frac{d\,\mathrm{N}_{w\,i}}{dx}\frac{dN_{\psi\,j}}{dx}(\frac{dw}{dx})dx \end{cases} \tag{35b}$$

$$\begin{cases} K_{31}^{ij} = \int_{x_a}^{x_b} A_{11}^1 \frac{d\,\mathrm{N}_{\psi i}}{dx}\frac{d\,\mathrm{N}_{uj}}{dx}dx \\ K_{32}^{ij} = \int_{x_a}^{x_b} k_s\, B_{11}^0 N_{\psi i}\frac{\partial\,\mathrm{N}_{wj}}{\partial x}dx + \int_{x_a}^{x_b}(\mu+\frac{1}{2})A_{11}^1 \frac{d\,\mathrm{N}_{\psi\,i}}{dx}\frac{dN_{w\,j}}{dx}(\frac{dw}{dx})dx \\ K_{33}^{ij} = \int_x k_s\, B_{11}^0\, \mathrm{N}_{\psi\,i}N_{\psi\,j}dx + \int_x A_{11}^2 \frac{d\,\mathrm{N}_{\psi i}}{dx}\frac{d\,\mathrm{N}_{\psi\,j}}{dx}dx \end{cases} \tag{35c}$$

- Mass matrix

$$\begin{cases} M_{11}^{l} = \int_{x_a}^{x_b} I_0 N_{u\,i}N_{u\,j}\,dx \quad , M_{12} = 0,\ M_{13}^{l} = \int_{x_a}^{x_b} I_1 N_{u\,i}N_{\psi\,j}dx \\ M_{21} = 0,\ M_{22}^{l} = \int_{x_a}^{x_b} I_0\ N_{w\,i}\ N_{wj}dx\,, M_{23} = 0 \\ M_{31}^{l} = \int_{x_a}^{x_b} I_1 N_{\psi i}N_{uj}dx\,, M_{32} = 0, M_{33}^{l} = \int_{x_a}^{x_b} I_2 N_{\psi i}N_{\psi\,j}dx \end{cases} \tag{36}$$

where

$$\begin{aligned} A_{11}^{i} &= b\int_{-\frac{h}{2}}^{\frac{h}{2}} z^{\,i} c_{11}(\mathrm{z})dz\ ,\ i = 0,1,2 \\ B_{11} &= \mathrm{b}\int_{-\frac{h}{2}}^{\frac{h}{2}} z^{\,i} G(\mathrm{z})dz\,,\ i = 0,1,2 \end{aligned} \tag{37a}$$

$$I_0 = b\int_{-\frac{h}{2}}^{\frac{h}{2}} p(z)dz\,,\ I_1 = b\int_{-\frac{h}{2}}^{\frac{h}{2}} z\ p(z)dz\,,\ I_2 = b\int_{-\frac{h}{2}}^{\frac{h}{2}} z^{\,2}\,p(z)dz \tag{37b}$$

4. Numerical results and discussions

In this paper, the nonlinear static and free vibration analysis of Euler-Bernoulli composite beam

Table1 The geometrical, mechanical and physical parameters of Euler-Bernoulli composite beam model reinforced by CNTs (Yas and Heshmati 2012)

Parameter	Value	Parameter	Value	Parameter	Value
E_m	10 GPa	E_{CNT}	649.12 GPa	L	5 m
P_m	1150 (kgm^{-3})	P_{CNT}	1400 (kgm^{-3})	$b=h$	0.1 m

Table 2 The effect of various boundary conditions on the dimensionless nonlinear deflection of nano-composite beam for $q=1000\frac{N}{m}$

Various BC's	Distribution types of FG-SWCNTs	L/h=10	L/h=20	L/h=30	L/h=40	L/h=50	L/h=60
C-C	UD	3.1414e-06	2.5131e-05	8.4818e-05	2.0103e-04	3.9237e-04	6.7627e-04
	SFG	2.1669e-06	1.7335e-05	5.8506e-05	1.3867e-04	2.7079e-04	4.6753e-04
	USFG	4.0115e-06	3.2095e-05	1.0835e-04	2.5703e-04	5.0237e-04	8.6681e-04
C-S	UD	6.2829e-06	5.0263e-05	1.6962e-04	4.0172e-04	7.8097e-04	1.3262 -03
S-S	UD	1.5707e-05	1.2565e-04	4.2365e-04	9.9502e-04	1.859e -03	2.8509 e-03
S-H	UD	1.5707e-05	1.2566 e-04	4.2406 e-04	1.0044e-03	1.9530e-03	3.3202e-03

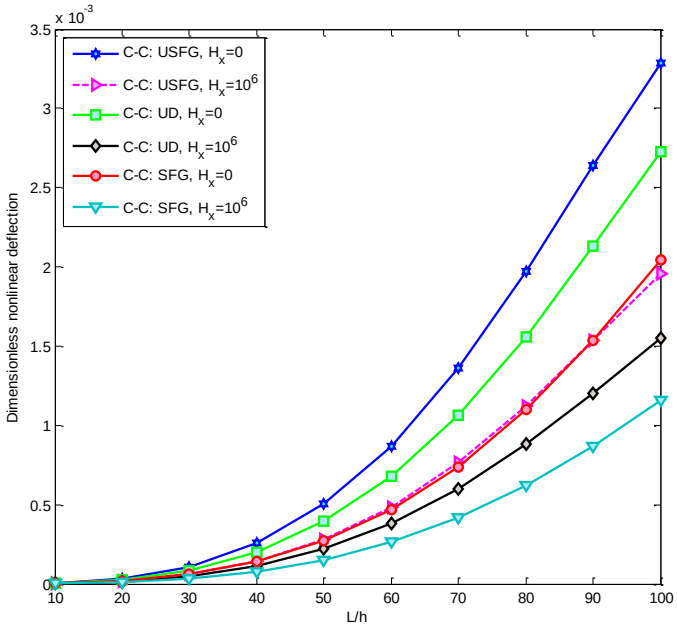

Fig. 2 Effects of aspect ratio (L/h) and magnetic field on the dimensionless nonlinear deflection for various distributions of nanotubes

model reinforced by FG-SWCNTs with geometrical imperfection under uniformly distributed load using FEM is investigated. The physical, geometrical and mechanical parameters of Euler-Bernoulli composite beam model reinforced by CNTs are considered in Table 1.

4.1 Static analysis

In this part, the effect of geometrical imperfection and UD, USFG and SFG distributions of CNT on the axial non-dimensional deflection of beam is taken into account. Table 2 and Fig. 2 depict the effect of various boundary conditions on the dimensionless nonlinear deflection of Euler-Bernoulli composite beam model reinforced by FG-SWCNTs for different boundary conditions. In this Table, letter C, S and H denote clamped, simply supported and hinged boundary conditions in the edge of the composite beam, respectively. According to Table 2 and Fig. 2, the dimensionless nonlinear deflection increases with an increase in the aspect ratio (L/h); also it is obvious that the nano-composite beam is stiffer as reinforced by SFG distribution type rather than other distribution types. It is shown from this figure that with considering magnetic field, the Euler-Bernoulli composite beam model reinforced by FG-CNT becomes stiffer, thus the dimensionless nonlinear deflection decreases for this state.

Fig. 3 shows the non-dimensional nonlinear transverse deflection of nano-composite beam for different boundary conditions and the fixed geometrical defects. It can be seen from Fig. 3 that by increasing uniformly distributed load, the dimensionless nonlinear displacement increases. From this figure S-H beam deforms more as expected than other states. Moreover, it is concluded that with considering S-H boundary condition, the nano-composite beam becomes more flexible with respect to the other boundary conditions. Also, the clamped boundary condition with respect to simply supported and hinged free boundary conditions leads to increase stiffer of the Euler-Bernoulli composite beam model. According to this figure with increasing uniformly distributed load of nano-composite beam, the difference of dimensionless nonlinear deflection between four cases increases; so the number of iterations for convergence system increases.

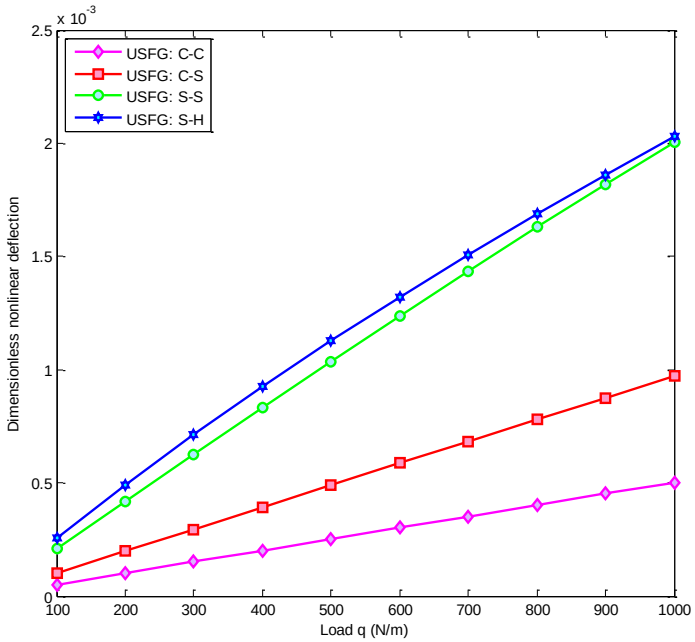

Fig. 3 The effect of various boundary conditions on the dimensionless maximum nonlinear deflections of nano-composite beam for μ=0.2 and L/h=50

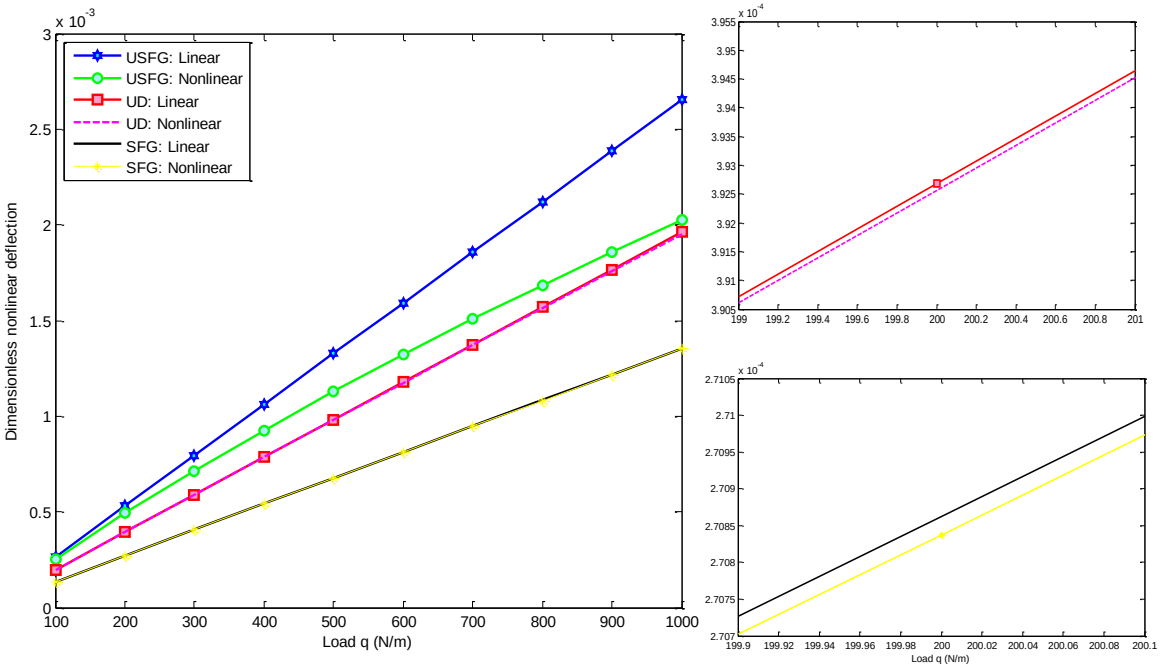

Fig. 4 The effect of various distributions of CNTs including UD, USFG and SFG on the dimensionless maximum deflection of nano-composite beam for μ=0.2 and L/h=50

The effect of various distributions of CNTs including UD, USFG and SFG on the transverse deflection of Euler-Bernoulli composite beam model reinforced by FG-CNTs under different loadings for S-H boundary condition and L/h=50 is shown in Fig. 4. The results show that, the dimensionless nonlinear deflection of USFG nano-composite beam is more than other states. So one can be expressed SFG beam is stiffer than the other state. Also it can be seen that the deference between linear and nonlinear dimensionless deflection response for USFG beam is more than the other state and this difference between two cases increases by increasing aspect ratio (L/h).

Figs. 5(a)-(b) depict the dimensionless nonlinear maximum deflection and nonlinear to linear maximum deflection ratio for S-H boundary conditions and L/h=50 in terms of the uniformly distributed load for various waviness at USFG state, respectively. It can be seen from Figs. 5(a) and 5(b) that the magnitudes of the transverse deflection decrease with an increase in the values of the waviness. Moreover, as the amplitude of waviness increases, the dimensionless nonlinear deflection of nano-composite beam is more sensitive to the von Karman type nonlinearity $(\frac{\partial w}{\partial x})^2$ in Eq. (9). In the other hands, the difference between curves for various amplitude of waviness in Fig. 5(b) is more than that of in Fig. 5(a). It is illustrated from Fig. 5(a) that the dimensionless nonlinear maximum deflection increases with an increase in the uniformly distributed load, while for dimensionless nonlinear to linear maximum deflection ratio is vice versa in Fig. 5(b).

Fig. 6 shows the effect of length-to-thickness ratio on the transverse deflections of Euler-Bernoulli composite beam model is presented. It is shown that as the beam becomes thicker at a special length; its curves are closer to linear state, while thin beam shows nonlinearity more

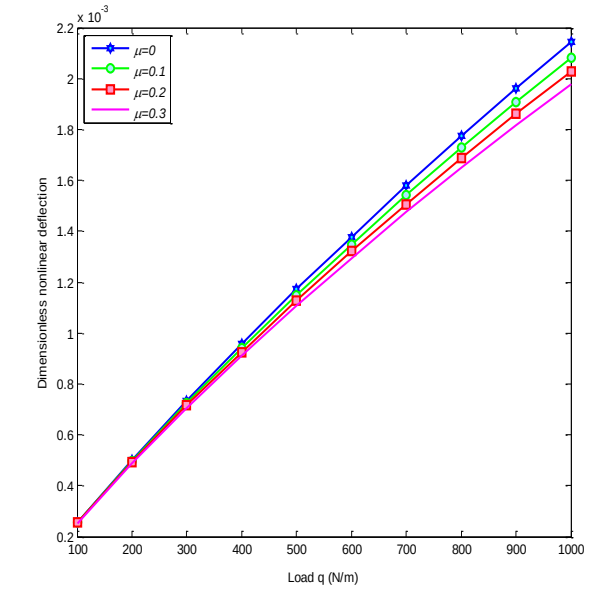

(a)

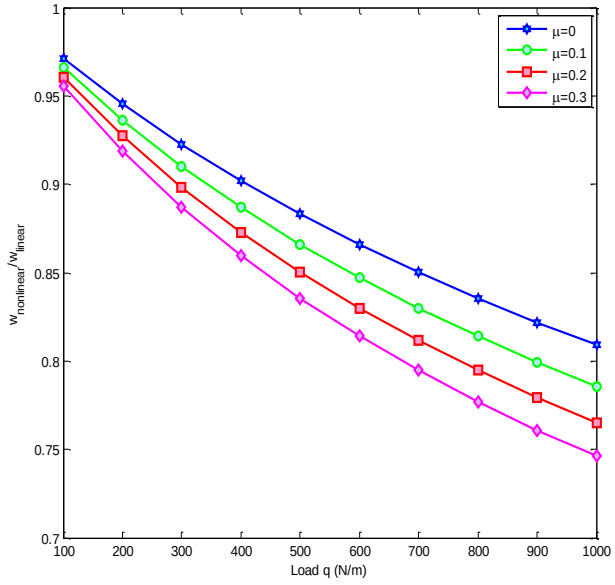

(b)

Fig. 5 The effect of various waviness on (a) the dimensionless nonlinear maximum deflection (b) dimensionless nonlinear to linear maximum deflection for S-H boundary condition and *L/h*=50

strongly. Also it is clear that the dimensionless nonlinear deflection of the nano-composite beam reduces as the aspect ratio (*h/L*) increases, which makes the beam stiffer.

Figs. 7(a)-(b) depict the good agreement between the obtained results by FEM (ten elements) and exact solution of the isotropic EBBT for S-S and C-C boundary conditions, respectively, and *L/h*=50. These figures show that the C-C and S-S boundary conditions are satisfied as well as for

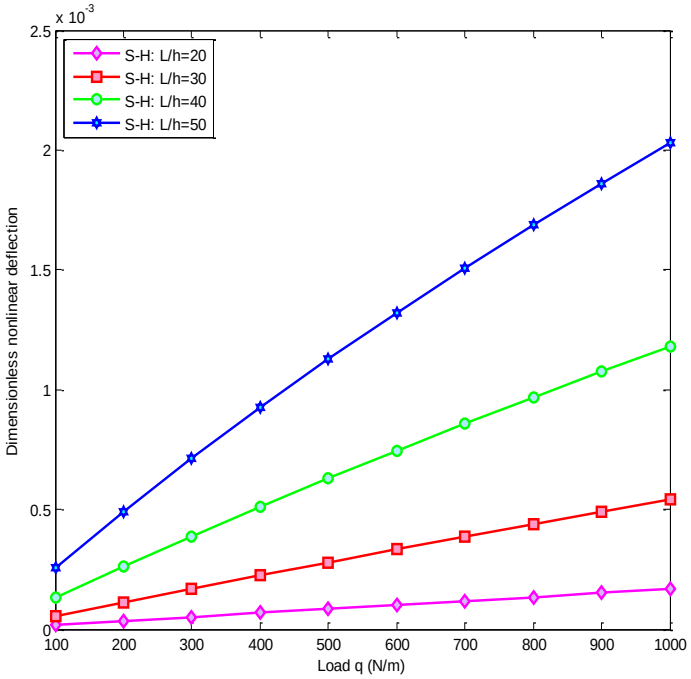

Fig. 6 Dimensionless nonlinear maximum deflection-load curves for μ=0.2 and USFG nano-composite beam for various values of the aspect ratio

two theories. According to (Reddy 2004), Young's modulus, geometric properties of beam is considered as E=30e6 Psi, P=1 *lb/in*, L=50 *in*, b=h=1 *in*.

Exact solutions of isotropic Euler-Bernoulli beam theory for C-C and S-S boundary conditions are given by

C-C: $$u_0(x)=0 \ , \quad w_0(x)=\frac{q_0 L^4}{24 D_{xx}}\left(\frac{x}{L}\right)^2\left(1-\frac{x}{L}\right)^2 \tag{38a}$$

S-S: $$u_0(x)=0 \ , \quad w_0(x)=\frac{q_0 L^4}{24 D_{xx}}\left(\frac{x}{L}-2\left(\frac{x}{L}\right)^3+\left(\frac{x}{L}\right)^4\right) \tag{38b}$$

4.2 Free vibration analysis

In this part, the effects of the various distributions of SWCNTs and variation boundary condition on non-dimensional natural frequency are discussed. Also the influence of various amplitude of the waviness on the dimensionless natural frequency is presented. The dimensionless natural frequency is computed as follows

$$\Omega=\omega L\sqrt{\frac{\rho_m}{E_m}} \tag{39}$$

Dimensionless natural frequency is computed using FEM for the Euler-Bernoulli composite

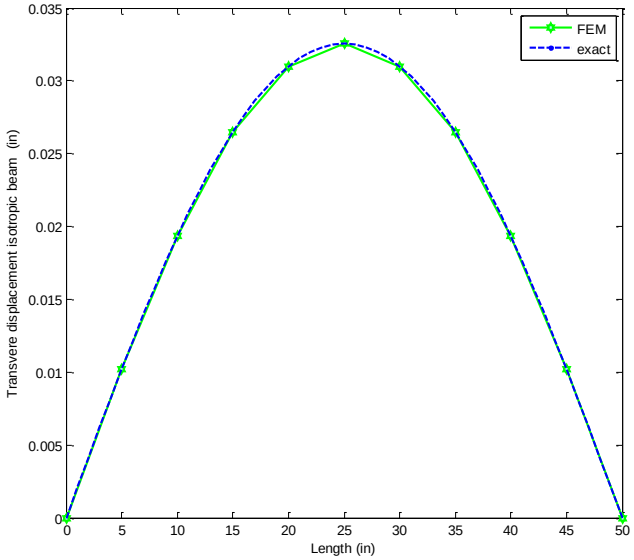

(a) simply-simply

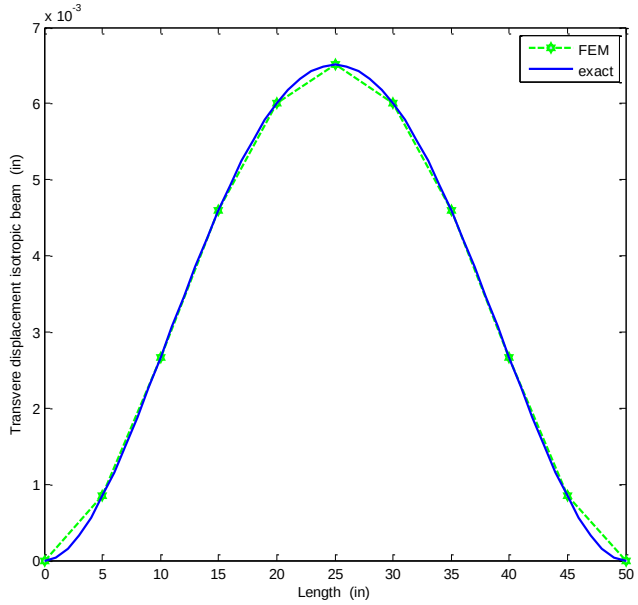

(b) clamped-clamped

Fig. 7 Deformed shapes of the beam for (a) simply-simply and (b) the clamped-clamped boundary conditions

beam model with various boundary conditions and the obtained results are listed in Table 3. According to (Eltaher *et al*. 2013), Young's modulus, density, and geometric properties of beam is considered as $E=30GPa, \rho=1\frac{kg}{m^3}$, $L/h=10$. In this Table, the obtained natural frequencies from the present work (FEM) of the Euler-Bernoulli composite beam model are compared with the results

Table 3 Comparison between the results of the present work (FEM) and the obtained results by Eltaher *et al*. (2013)

Various boundary condition	Present work	Eltaher *et al*. 2013
C-C	22.4404	22.4926
S-S	9.9089	9.9106
C-S	15.4693	15.4937
C-F	3.5376	3.5228

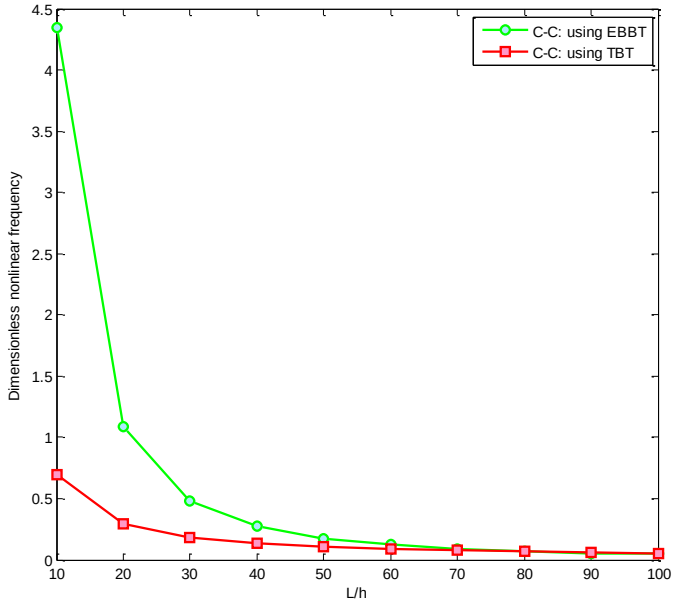

Fig. 8 The dimensionless nonlinear frequency of composite beam reinforced by UD-CNTs using TBT and EBBT versus *L/h* for C-C boundary conditions

available in the literature (Eltaher *et al*. 2013). From Table 3, one can be observed that the present results are in good agreement with the obtained results by (Eltaher *et al*. 2013) for various boundary conditions.

Fig. 8 depicts the dimensionless nonlinear frequency of composite beam reinforced by UD-CNTs using the Timoshenko and Euler-Bernoulli beam theories (TBT and EBBT) versus the aspect ratio (*L/h*) for C-C boundary conditions. It can be concluded that the difference between the dimensionless nonlinear frequency predicted by EBBT and TBT is negligible for *L/h*>50. This is due to the fact that the shear stress effect is negligible for long nanotubes.

Figs. 9(a)-(b) and Table 4 indicate the non-dimensional linear and nonlinear natural frequency of C-C nano-composite beam for three types of CNT distributions. Increasing the aspect ratio (*h/L*) leads to increase the dimensionless natural frequency for UD, USFG and SFG beam. Also at the specified value of (*h/L*), the dimensionless natural frequency for SFG beam is more than the other state. It means that the USFG beam causes to decrease the first natural frequency. Also it can be seen that the difference between linear and nonlinear natural frequency response for USFG beam is more than the other state.

Table 4 Effects of (*h/L*) and various distribution of CNT on the natural frequency for C-C boundary conditions of nano-composite beam reinforced by CNT

	CNT	*h/L*=0.05	0.06	0.07	0.08	0.09	0.1
Linear Solution	UD	0.50219726	0.60255180	0.70286011	0.80311447	0.90330728	1.00343089
	USFG	0.42956977	0.51540083	0.60118672	0.68691998	0.77259314	0.858198759
	SFG	0.60466788	0.72549772	0.84627105	0.96697850	1.08761072	1.208158407
Nonlinear Solution	UD	0.50229990	0.60258047	0.70286985	0.80311831	0.90330896	1.00343170
	USFG	0.46089357	0.53527270	0.61428161	0.69590200	0.77898367	0.862892205
	SFG	0.60470847	0.72550906	0.84627491	0.96698001	1.08761139	1.208158725

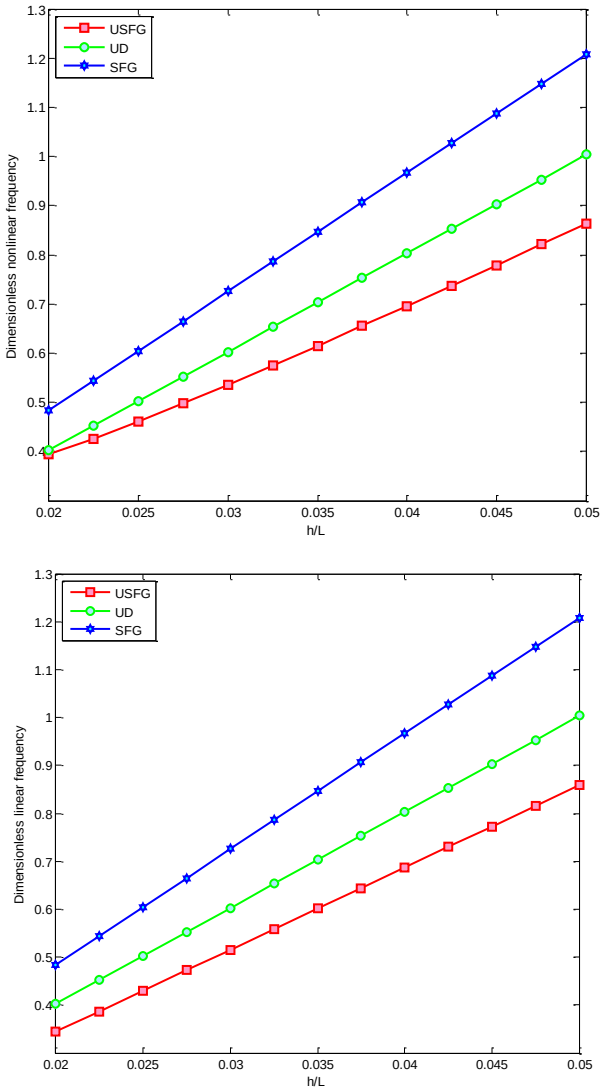

Fig. 9 The effect of various distributions of CNTs on (a) dimensionless nonlinear natural frequency (b) dimensionless linear natural frequency

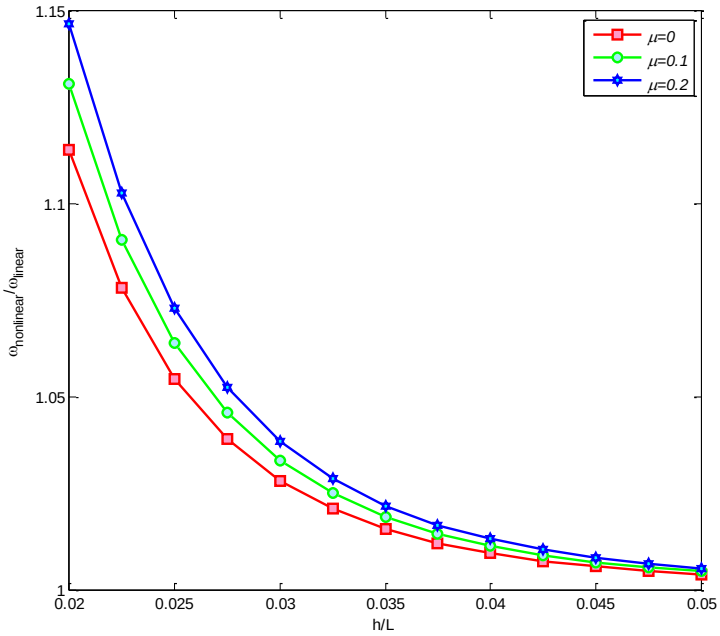

Fig. 10 The effect of waviness amplitude on the dimensionless nonlinear to linear natural frequency ratio for USFG composite beam

The influences of aspect ratio (*h/L*) on the nonlinear to linear natural frequency ratio for different amplitudes of the waviness USFG nano-composite beam and C-C boundary conditions are shown in Fig.10. According to this figure, the frequency ratio decreases with an increase of aspect ratio. Also, with increasing amplitude of the waviness, the natural frequency ratio increases. Moreover, the stiffness of structure reinforced by CNTs increases with considering the waviness amplitude. Also, it is shown from the results that the effect of waviness amplitude on the system is nonlinear. On the other hands, with increasing this parameter, the nonlinear stiffness of system increases while the rigidity of linear system does not change.

Fig. 11 shows the influence of various boundary conditions on the frequency ratio. It can be observed that the natural frequency ratio of USFG composite beam for C-C boundary conditions is more than the other state. On the other hands, the C-C boundary condition leads to increase more the stiffness of composite beam reinforced by FG-CNTs with respect to the other state.

It is known that for linear modal analysis, it is now possible to what the linear natural frequencies for Euler-Bernoulli composite beam are. In this case, the linear natural frequencies come from $[M^{-1}][k_{linear}]$ according to Eqs. (32)-(34). However, Eq. (33) has additional, coupled, and nonlinear terms (that are obtained from the geometrical nonlinear von Karman's kinematic equations with initial geometrical imperfection (Eq. (9)) which will mean, in practice, that the natural frequencies are not the same as the linear ones.

It is also possible that the nonlinear coupling terms may cause additional resonances in the composite beam model, which cannot be predicted by the linear equations. For example, sub-harmonic resonance is a form of nonlinear resonance and also, other types of nonlinear resonance phenomena include parametric and auto-parametric resonance. In this research, the nonlinear natural frequencies are obtained by nonlinear FEM solutions.

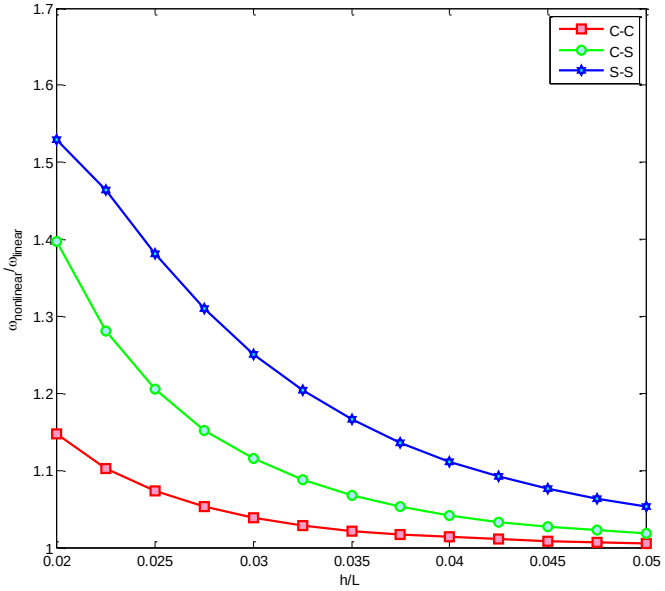

Fig. 11 The effect of various boundary conditions on the dimensionless nonlinear to linear natural frequency ratio for μ=0.2 and USFG composite beam

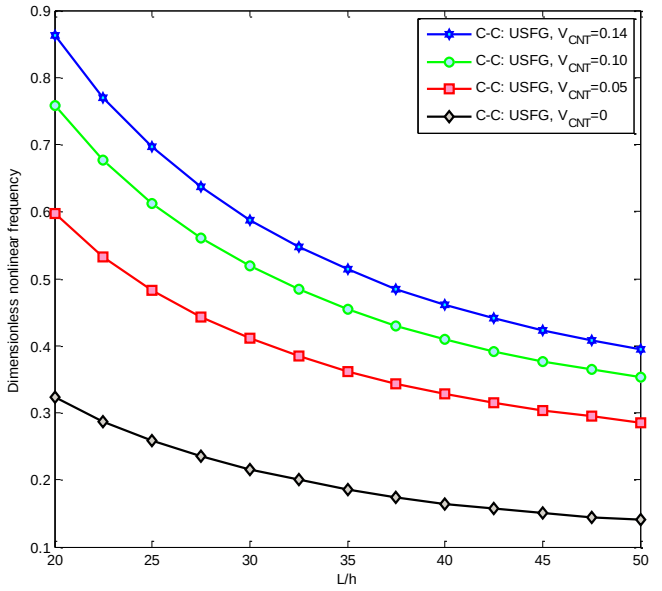

Fig. 12 The effect of various volume fraction of USFG-CNT on the dimensionless nonlinear natural frequency for μ=0.2 and C-C boundary conditions

This point has been shown in Figs. 10 and 11, that in lower *h/L* (or higher *L/h*), the difference between nonlinear and linear natural frequency is noticeable.

Fig. 12 and Table 5 indicate the effect of various volume fraction of USFG-CNT on the

Table 5 The effects of various volume fraction of USFG-CNT on the dimensionless nonlinear natural Frequency for C-C boundary condition and μ=0.2

L/h	20	*R*	30	*R*	40	*R*	50	*R*
V_{CNT}=0	0.3229	-	0.2159	-	0.1646	-	0.1401	-
V_{CNT}=0.05	0.5965	84.69	0.4108	90.27	0.3282	99.37	0.2858	104.097
V_{CNT}=0.10	0.7581	134.75	0.5184	140.12	0.4095	148.73	0.3528	151.88
V_{CNT}=0.14	0.8629	167.16	0.5876	172.17	0.4609	179.95	0.3942	181.43

dimensionless nonlinear natural frequency for μ=0.2 and C-C boundary conditions. It is shown that with increasing the volume fraction of USFG-CNT, the dimensionless nonlinear natural frequency increases. Moreover, the considering volume fraction of FG-CNT leads to enhance the stiffness of structure. The *R* parameter is defined as the relative increasing percentage of dimensionless nonlinear natural frequency for various volume fractions of USFG-CNT that is illustrated in Table 5. It is concluded that the *R* parameter increases with increasing of volume fraction while the rate of this parameter decreases. Thus one can be obtained the optimum value of USFG-CNT volume fraction to prevent from resonance phenomenon.

5. Conclusions

In this paper, the nonlinear static and free vibration analysis of Euler-Bernoulli composite beam model reinforced by FG-SWCNTs with geometrical imperfection under uniformly distributed load using FEM is studied. The effects of variation values of μ, UD, USFG, SFG distributions of CNT on the nonlinear displacements and natural frequency are illustrated. Also the influence of various loading and boundary conditions on the dimensionless nonlinear deflection and natural frequency is studied. Meanwhile the obtained results are in good agreement with the reported results by Eltaher *et al*. (2013) for various boundary conditions. The result of this research can be listed as follows:

1. With increasing value of the waviness, the non-dimensional nonlinear frequency ratio increases for UD, SFG and USFG beam.
2. For the same loading, the dimensionless nonlinear deflection for USFG beam is more than the other state. So one can be expressed SFG beam is stiffer than the other state.
3. The dimensionless normalized deflection of FG nano-composite Euler-Bernoulli beam for pinned-hinged boundary condition is more than the other states.
4. At the specified value of μ, the dimensionless nonlinear deflection of USFG beam is more than the other state.
5. Euler-Bernoulli beam becomes stiffer with increasing aspect ratio (*h/L*) and the non-dimensional deflection the beam reduces.
6. The specified value of aspect ratio, the dimensionless natural frequency for SFG beam is more than the other state.
7. The natural frequency ratio of USFG nano-composite beam for C-C boundary conditions is more than the other state. On the other hands, the C-C boundary condition leads to increase more the stiffness of composite beam reinforced by FG-CNTs with respect to the other state.
8. It can be concluded that the difference between the dimensionless nonlinear frequency

predicted by EBBT and TBT is negligible for L/h>50. This is due to the fact that the shear stress effect is negligible for long nanotubes.

9. It is shown that with increasing the volume fraction of USFG-CNT, the dimensionless nonlinear natural frequency increases. On the other hands, the stiffness of structure increases with the considering volume fraction of FG-CNT.

10. It is concluded that the R parameter increases with increasing of volume fraction while the rate of this parameter decreases. Thus one can be obtained the optimum value of USFG-CNT volume fraction to prevent from resonance phenomenon.

Acknowledgments

The authors would like to thank the referees for their valuable comments. They are also grateful to the Iranian Nanotechnology Development Committee for their financial support and also grateful to the University of Kashan for supporting this work by Grant No. 363452/14.

References

Akbas, S.D. (2015), "Large deflection analysis of edge cracked simple supported beams", *Struct. Eng. Mech*., **54**(3), 433-451

Ansari, R. and Ramezannezhad, S. (2011), "Nonlocal Timoshenko beam model for the large-amplitude vibrations of embedded multiwalled carbon nanotubes including thermal effects", *Physica. E.*, **43**, 1171-1178.

Bouiadjra, B.B., Bedia, E.A. and Tounsi, A. (2013), "Nonlinear thermal buckling behavior of functionally graded plates using an efficient sinusoidal shear deformation theory", *Struct. Eng. Mech.*, **48**(4), 547-567.

Eltaher, M.A., Abdelrahman, A.A., Al-Nabawy, A., Khater, M. and Mansour, A. (2014), "Vibration of nonlinear graduation of nano-Timoshenko beam considering the neutral axis position", *Appl. Math. Comput*., **235**,512-529.

Eltaher, M.A., Alshorbagy, A.E. and Mahmoud, F.F. (2013), "Vibration analysis of Euler-Bernoulli nanobeams by using finite element method", *Appl. Math. Model.*, **37**, 4787-4797.

Farshidianfar, A. and Soltani, P. (2012), "Nonlinear flow-induced vibration of a SWCNT with a geometrical imperfection", *Comput. Mater. Sci*., **53**, 105-116.

Ghorbanpour Arani, A., Atabakhshian, V., Loghman, A., Shajari, A.R. and Amir, S. (2012),"Nonlinear vibration of embedded SWBNNTs based on nonlocal Timoshenko beam theory using DQ method", *Physica B.*, **407**, 2549-2555.

Heshmati, M. and Yas, M.H. (2013), "Vibrations of non-uniform functionally graded MWCNTs-polystyrene nano-composite beams under action of moving load", *Mater. Des.*, **46**, 206-218.

Lau, K.T., Gu, C., Gao, G.H., Ling, H.Y. and Reid, S. (2004), "Stretching process of single and multiwalled carbon nanotubes for nanocomposite", A*ppl. Carbon*., **42**, 8-426.

Li, C. (2013), "Size-dependent thermal behaviors of axially traveling nanobeams based on a strain gradient theory", *Struct. Eng. Mech.*, **48**(3), 415-434.

Li, Z.M. (2014), "Thermal post buckling behavior of 3D braided beams with initial geometric imperfection under different type temperature distributions", *Compos. Struct.*, **108**, 924-936.

Liew, K.M., Lei, Z.X. and Zhan, L.W. (2015), "Mechanical analysis of functionally graded carbon nanotube reinforced composites", *A Review, Compos. Struct.*, **120**,90-97.

Mohammadimehr, M. and Mostafavifar, M. (2016), "Free vibration analysis of sandwich plate with a transversely flexible core and FG-CNTs reinforced nanocomposite face sheets subjected to magnetic field and temperature-dependent material properties using SGT", *Compos. Part B: Eng.*, **94**(1), 253-270.

Mohammadimehr, M. and Rahmati, A.H. (2013), "Small scale effect on electro-thermo-mechanical vibration analysis of single-walled boron nitride nanorods under electric excitation", *Turk J. Eng. Environ. Sci.*, **37**, 1-15.

Mohammadimehr, M., Mohandes, M. and Moradi, M. (2016a), "Size dependent effect on the buckling and vibration analysis of double-bonded nanocomposite piezoelectric plate reinforced by boron nitride nanotube based on modified couple stress theory", *J.Vib. Control*, **22**(7), 1790-1807.

Mohammadimehr, M., Monajemi, A.A. and Moradi, M. (2015a), "Vibration analysis of viscoelastic tapered micro-rod based on strain gradient theory resting on visco-pasternak foundation using DQM", *J. Mech. Sci. Technol.*, **29**(6), 2297-2305.

Mohammadimehr, M., Rousta Navi, B. and Ghorbanpour Arani, A. (2015b), "Free vibration of viscoelastic double-bonded polymeric nanocomposite plates reinforced by FG-SWCNTs using MSGT, sinusoidal shear deformation theory and meshless method", *Compos. Struct.*, **131**, 654-671.

Mohammadimehr, M., Salemi, M. and Rousta Navi, B. (2016b), "Bending, buckling, and free vibration analysis of MSGT microcomposite Reddy plate reinforced by FG-SWCNTs with temperature-dependent material properties under hydro-thermo-mechanical loadings using DQM", *Compos. Struct.*, **138**, 361-380.

Narendar, S., Gupta, S.S. and Gopalakrishnan, S. (2012), "Wave propagation in single-walled carbon nanotube under longitudinal magnetic field using nonlocal Euler-Bernoulli beam theory", *Appl. Math. Model.*, **36**, 4529-4538.

Putcha, N.S. and Refined, A. (1986), "Mixed shear flexible finite element for the nonlinear analysis of laminated plates",*Comput. Struct.*, **22**, 529-538.

Rahmati, A.H. and Mohammadimehr, M. (2014), "Vibration analysis of non-uniform and non-homogeneous boron nitride nanorods embedded in an elastic medium under combined loadings using DQM", *Physica B.*, **440**, 88-98.

Ranjan, R. (2011), "Nonlinear finite element analysis of bending of straight beams using hp-spectral approximations", *J. Solid. Mech*., **3**, 96-113.

Reddy, J.N. (1987),"Mixed finite element models for laminated composite plate", *J. Eng. Indus.*, **109**, 39-45.

Reddy, J.N. (2004), *An Introduction to nonlinear finite element analysis*, Oxford University Press, Oxford, New York, USA.

Şimşek, M. (2014), "Nonlinear static and free vibration analysis of microbeams based on the nonlinear elastic foundation using modified couple stress theory and He's variational method", *Compos. Struct.*, **12**, 264-272.

Wang, B., Deng, Z., Ouyang, H. and Zhou, J. (2015), "Wave propagation analysis in nonlinear curved single-walled carbon nanotubes based on nonlocal elasticity theory", *Physica. E.*, **66**, 283-292.

Wang, B., Deng, Z.C. and Zhang, K. (2013), "Nonlinear vibration of embedded single walled carbon nanotube with geometrical imperfection under harmonic load based on nonlocal Timoshenko beam theory", *Appl. Math. Mech., Engl. Ed. (English Edition)*, **34**(3), 269-280.

Yas, M.H. and Heshmati, M. (2012), "Dynamic analysis of functionally graded nanocomposite beams reinforced by randomly oriented carbon nanotube under the action of moving load", *Appl. Math. Model.*, **36**, 1371-1394.

Yas, M.H. and Samadi, N. (2012), "Free vibrations and buckling analysis of carbon nanotube-reinforced composite Timoshenko beams on elastic foundation", *Int. J. Press. Ves. Pip*., **98**, 119-128.